Experimental scaling law for mass ablation rate from a Sn plasma generated by a 1064 nm laser

Russell A. Burdt,[1,2,a)] Sam Yuspeh,[1,2] Kevin L. Sequoia,[1] Yezheng Tao,[1] Mark S. Tillack,[1] and Farrokh Najmabadi[1,2]
[1]*Center for Energy Research, University of California San Diego, La Jolla, California 92093-0417, USA*
[2]*Electrical and Computer Engineering, University of California San Diego, La Jolla, California 92093-0407, USA*

(Received 5 May 2009; accepted 1 July 2009; published online 10 August 2009)

The ablation depth in planar Sn targets irradiated with a pulsed 1064 nm laser was investigated over laser intensities from 3×10^{11} to 2×10^{12} W/cm^2. The ablation depth was measured by irradiating a thin layer of Sn evaporated onto a Si wafer, and looking for signatures of Si ions in the expanding plasma with spectroscopic and particle diagnostics. It was found that ablation depth scales with laser intensity to the (5/9)th power, which is consistent with analytical models of steady-state laser ablation, as well as empirical formulae from previous studies of mass ablation rate in overlapping parameter space. In addition, the scaling of mass ablation rate with atomic number of the target as given by empirical formulae in previous studies using targets such as C and Al, are shown to remain valid for the higher atomic number of the target ($Z=50$) used in these experiments. © *2009 American Institute of Physics*.
[DOI: 10.1063/1.3190537]

I. INTRODUCTION

Laser produced Sn plasma, in its role as an efficient extreme ultraviolet (EUV) x-ray source, is being studied extensively to support the commercial development of EUV lithography, which will enable the next generation of integrated circuits with feature sizes of 22 nm.[1] Tin plasma heated to a few tens of eV has many thousands of emission lines centered at 13.5 nm, which is the wavelength of choice for EUV lithography at which available multilayer Mo/Si x-ray optics are highly reflective at normal incidence.[2] Of significant interest in these experiments is the ablation dynamics of the Sn target. Specifically, the ablation rate of mass from the target is a factor controlling the minimum amount of mass required per target as well as the debris emitted from the plasma, both of which are significant concerns in the development of the application.[3,4] In addition, the scaling of ablation rate with laser intensity provides insight into the laser absorption and energy transport physics,[5] and may also aid in the benchmarking of radiation hydrodynamics codes used in EUV source development.

Extensive research has been conducted to determine the scaling of mass ablation rate with laser intensity for the laser fusion application, at which typical laser wavelengths are 1.06 μm and its three harmonics, typical laser intensities range from approximately 10^{12} to 10^{15} W/cm^2, and the atomic number of the targets used range from 1 to 14 (H to Si).[6–9] Minimal research has been conducted in the context of the EUV lithography application,[10] in which typical laser wavelengths are 1.064 and 10.6 μm, and typical intensities range from approximately 10^{10} to 10^{12} W/cm^2, overlapping the low end of parameter space in the laser fusion application. Selected results of these previous studies are summarized in Table I. It is seen that for laser intensities above 10^{13} W/cm^2 the mass ablation rate scales as $\dot{m}\propto I_a^{1/3}\lambda_L^{-4/3}$, whereas for laser intensities below 10^{13} W/cm^2 the mass ablation rate scales as $\dot{m}\propto I_a^{5/9}\lambda_L^{-4/9}$, where $\dot{m}$ is the mass ablation rate, λ_L is the laser wavelength, and I_a is the absorbed laser intensity, which for the laser produced plasmas relevant to EUV lithography is equal to the laser intensity due to strong inverse bremsstrahlung absorption.[11] The scaling law at higher intensity is consistent with a model of steady-state planar ablation in which collisional absorption at the critical surface dominates, and the energy transport from the critical surface to the ablation front is inhibited to a small fraction of the free-streaming limit.[5,12] At lower laser intensities relevant to the EUV lithography application, the scaling is consistent with a model of steady-state planar ablation in which energy deposition occurs by nonlocalized collisional absorption before the critical density, and the energy transport to the ablation front is by diffusive conduction of thermal electrons.[5,13]

In the present work, the ablation depth was measured using a 1064 nm neodymium-doped yttrium aluminum garnet (Nd:YAG) laser at four different laser intensities, from 3×10^{11} to 2×10^{12} W/cm^2, which overlap the laser intensities used by Ng *et al.*[7] and by Dahmani and Kerdja.[9] The targets were made by evaporating a thin layer of Sn onto a Si wafer, and the ablation depth was measured by irradiating targets with progressively thicker layers of Sn until the signatures of Si ions in the expanding plasma disappeared. Three diagnostics were used to directly and indirectly measure the presence of Si ions in the expanding plasma—a calibrated EUV energy monitor, an EUV spectrometer, and an electrostatic ion energy analyzer. It was found that ablation depth scales with laser intensity to the (5/9)th power, consistent with the results of Ng *et al.*[7] and Dahmani and Kerdja.[9] If the scaling of mass ablation rate with laser wave-

a)Electronic mail: russellburdt@yahoo.com.

TABLE I. Summary of selected scaling laws and numerical approximations for ablation rate found in the literature (Refs. 6–10). I_a is the absorbed laser intensity in $[10^{11}\ \mathrm{W/cm^2}]$, λ_L is the laser wavelength in $[\mu\mathrm{m}]$, $\dot{m}$ is the ablation rate in $[\mathrm{g/cm^2/s}]$, and Z is the target atomic number.

Reference	Wavelength (μm)	Laser pulse duration (ns)	Laser spot diameter (μm)	Laser intensity ($\mathrm{W/cm^2}$)	Target material and type	Ablation rate (numerical approximation if available)
Fabbro *et al.*[a]	1.06, 0.53, and 0.27	0.1–2.5	50–70	5×10^{13} to 10^{15}	CH, planar	$\dot{m}\approx(11\times10^3)I_a^{1/3}\lambda_L^{-4/3}$
Ng *et al.*	0.53, 0.35, and 0.27	2	80	10^{12} to 5×10^{13}	Al, planar	$\dot{m}\propto I_a^{5/9}\lambda_L^{-4/9}$
Dahmani[b]	1.06	0.7	44	10^{13} to 10^{15}	C and Si, planar	$\dot{m}\approx(5.5\times10^3)I_a^{1/3}\lambda_L^{-4/3}Z^{3/8}$
Dahmani and Kerdja[c]	1.06	3	96	10^{11} to 4.5×10^{12}	Al, planar	$\dot{m}\approx(3.5\times10^3)I_a^{5/9}\lambda_L^{-4/9}Z^{3/8}$
Fujioka *et al.*[d]	1.064	10	500	10^{11} only	Sn, spherical	$\dot{m}\approx(2.8\times10^3)I_a^{5/9}\lambda_L^{-4/3}$
Present work	1.064	6.5	56	3×10^{11} to 2×10^{12}	Sn, planar	$\dot{m}\approx(3.0\times10^3)I_a^{5/9}\lambda_L^{-4/9}Z^{3/8}$

[a]Reference 6.
[b]Reference 7.
[c]Reference 8.
[d]Reference 9.
[e]Reference 10.

length and target atomic number found in the previous study of Dahmani and Kerdja[9] in overlapping parameter space were applied to the present data, then it was found that the numerical approximations of mass ablation rate agreed to within 15%. This indicates the empirical formulae found in the previous studies of Dahmani and Kerdja[9] using targets such as C and Al remain valid for the higher atomic number of the target ($Z=50$) used in these experiments.

II. EXPERIMENTAL CONDITIONS AND DIAGNOSTICS

A Nd:YAG laser with a full width half maximum pulse duration of 6.5 ± 0.5 ns was focused onto a planar Sn target in a $1/e^2$ focal diameter of 56 ± 3 μm. Four laser intensities were investigated in the experiments by adjusting the laser energy with a waveplate and polarizing beamsplitter in four settings equal to 53.2 ± 11.0, 150.8 ± 8.7, 250.7 ± 10.8, and 352.7 ± 11.7 mJ. The energy of several laser pulses prior and subsequent to those used in collecting data were recorded with a pyroelectric energy monitor and used to calculate the mean value and error in the laser pulse energy. Additional error in the laser pulse energy was manifest from attempting to replicate the four energy settings when irradiating each target installed in the vacuum chamber, which was the most difficult at the lowest nominal laser energy where incremental rotations of the waveplate generated significant variations in the laser energy. Including all sources of error, the laser intensities investigated were 3.3 ± 1.1, 9.4 ± 1.8, 15.7 ± 2.7, and 22.0 ± 3.6 $[10^{11}\ \mathrm{W/cm^2}]$.

The targets were made using electron beam evaporation to deposit thin layers of Sn with nanometer precision onto Si wafers several hundred micrometers thick. The Sn layer thickness was monitored during deposition by a quartz crystal thickness monitor, and verified postdeposition with a stylus profiler. Thirteen targets were prepared for the experiments with Sn layer thicknesses from 10 to 500 nm, in addition to an uncoated target and a target with a Sn layer several micrometers thick, hereafter referred to as the thick target. Each target was installed in a vacuum chamber evacuated below 10^{-5} torr and irradiated three times at each laser intensity. The target was translated in the focal plane before each shot to provide a fresh surface.

The ablation depth was measured by irradiating layered targets with progressively thicker layers of Sn until the signatures of Si ions in the expanding plasma disappeared, indicating the ablation depth had been reached or exceeded. Silicon ions in the expanding plasma were measured directly and indirectly with three plasma diagnostics—a calibrated EUV energy monitor, an EUV spectrometer, and an electrostatic ion energy analyzer. Each diagnostic recorded data simultaneously with the others.

The calibrated EUV energy monitor[14] consists of a Zr filter, two multilayer Mo/Si mirrors, and an EUV photodiode aligned to the path of the expanding plasma. The integrated signal from the EUV photodiode is scaled by a calibration factor from the manufacturer (JenOptik) to obtain the EUV energy in a 2% bandwidth centered about 13.5 nm, hereafter referred to as the in-band emission. The total in-band emission over 2π sr is calculated from an assumed spatial distribution of EUV light and normalized to the laser energy to give the conversion efficiency (CE) of laser energy to in-band EUV light, which is a figure of merit for the EUV lithography application. The EUV spectrometer employs a 50 μm slit to collimate the radiation from the plasma onto a grating with 10^4 lines/mm. The dispersed light is then recorded by a cooled x-ray camera and sent to a computer for image processing. An indirect indication of Si ions in the expanding plasma is apparent from a CE measurement that is lower than, or a spectrum that is less intense than, similar measurements using the thick Sn target.

The electrostatic ion energy analyzer is a particle diagnostic, which is able to measure the presence of individual ion species in an expanding plasma by filtering the plasma in a radial electrostatic field into ions having a constant kinetic energy to charge state (KE/Z) ratio, and detecting these ions directly with a single channel electron multiplier.[15] Ions with different mass or different charge state meeting the filter criterion of the probe will arrive at the detector at different times, and a measurement of the current generated by the detector gives an indication of the number and types of ions present in the plasma meeting the filter criterion. A schematic of the experimental arrangement is shown in Fig. 1.

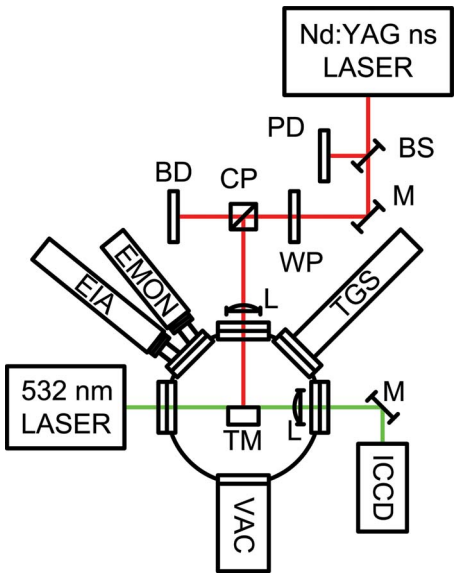

FIG. 1. (Color online) The experimental arrangement is shown. BS—beam sampler, PD—photodiode, WP—wave plate, CP—cube polarizer, BD—beam dump, L—lens, M—mirror, TM—target mount, VAC—vacuum pump, ICCD—intensified charge-coupled device camera used with 532 nm laser to align the target surface in the focal plane, TGS—transmission grating spectrometer installed at 45° with respect to target normal, EMON—calibrated EUV energy monitor installed at 39° with respect to target normal, and EIA—electrostatic ion energy analyzer installed at 51° with respect to target normal.

III. EXPERIMENTAL RESULTS

The data from the calibrated EUV energy monitor are collected into plots of CE as a function of target thickness at each of the four nominal laser intensities, as shown in Fig. 2. The curves are typically linear before the ablation depth, and saturate with some rolloff near the ablation depth. The horizontal lines in the figure represent the limiting values for CE obtained with the thick Sn target at each nominal laser intensity. The limiting value of CE is the highest at 3.3×10^{11} W/cm^2 and lowest at 2.2×10^{12} W/cm^2. The exact values at these laser intensities are consistent with previous work, which has investigated the optimal laser parameters for high CE, and the variation is due to enhanced reabsorption of in-band emission as laser intensity increases.[16,17] The author interpreted the ablation depth at each laser intensity to

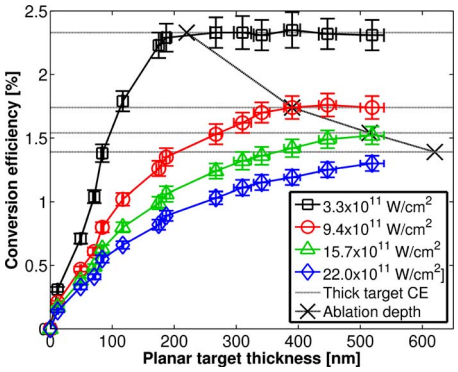

FIG. 2. (Color online) CE as a function of planar target thickness at each of the four nominal laser intensities.

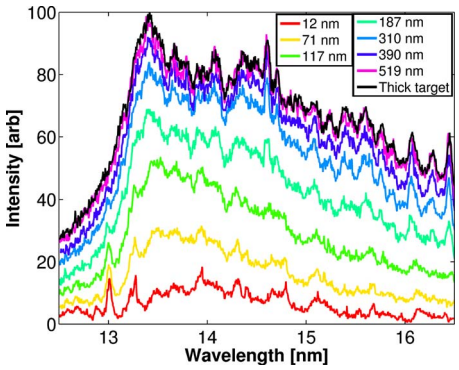

FIG. 3. (Color online) Evolution of the EUV spectrum at a laser intensity of 15.7 ± 2.7 [10^{11} W/cm^2] as the target thickness is increased.

equal 220, 390, 515, and 620 nm at the laser intensities 3.3 ± 1.1, 9.4 ± 1.8, 15.7 ± 2.7, and 22.0 ± 3.6 [10^{11} W/cm^2], respectively.

The data from the EUV spectrometer are collected into plots showing the evolution of the EUV spectrum at a constant laser intensity as the target thickness is increased. The target thickness at which the spectrum is as intense as the spectrum measured using the thick Sn target indicates the ablation depth has been reached or exceeded. For example, Fig. 3 shows the evolution of the EUV spectrum at the laser intensity 15.7 ± 2.7 [10^{11} W/cm^2] as the target thickness is increased. It is seen that when a target whose thickness is 519 nm is irradiated the EUV spectrum is as intense as the spectrum generated using the thick target, indicating the ablation depth has been reached at this target thickness. This is consistent with the measurement of ablation depth from the calibrated EUV energy monitor, as are the measurements of ablation depth using the EUV spectrometer at the three additional laser intensities.

The electrostatic ion energy analyzer can measure directly ions from both layers of a layered target whose thickness is less than the ablation depth. For example, Fig. 4 shows a time-of-flight waveform generated by the electrostatic ion energy analyzer in which three charge states of Sn and two charge states of Si meet the filter criterion of the probe. It was possible to measure ablation depth by looking for the target thickness at which ions from the base layer

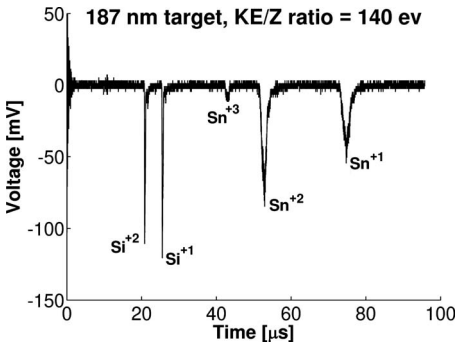

FIG. 4. Time-of-flight data generated by the electrostatic ion energy analyzer at a laser intensity of 9.4 ± 1.8 [10^{11} W/cm^2] using a 187 nm thick target. Each negative-going peak in the waveform represents the arrival of an ion species at the output of the probe meeting the filter criterion ($KE/Z = 140$ eV).

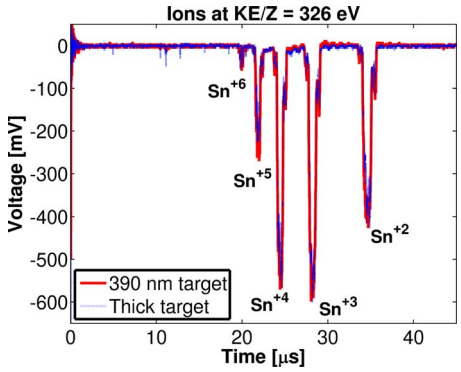

FIG. 5. (Color online) Time-of-flight data generated by the electrostatic ion energy analyzer at a laser intensity of 9.4 ± 1.8 [10^{11} W/cm^2] for the thick target and a 390 nm target. The signal levels are identical in both waveforms, indicating the ablation depth was reached.

were not recorded with the ion energy analyzer; however, this process was unrealistically time consuming because both the target thickness as well as the filter criterion of the probe had to be scanned at each laser intensity. A better method of measuring ablation depth with the electrostatic ion energy analyzer was to keep the filter criterion of the probe constant and scan the target thickness until the current generated by the probe was equal to that obtained using the thick target. For example, Fig. 5 shows the data from the electrostatic ion energy analyzer using the thick target and a 390 nm target at a laser intensity of 9.4 ± 1.8 [10^{11} W/cm^2], indicating the ablation depth has been reached. This result is consistent with the two spectroscopic diagnostics, as are the remaining measurements from the electrostatic ion energy analyzer.

IV. DISCUSSION

The spectroscopic and particle diagnostics used in the experiments generated consistent measurements of the ablation depth, i.e., d_a=220, 390, 515, and 620 nm at laser intensities of 3.3 ± 1.1, 9.4 ± 1.8, 15.7 ± 2.7, and 22.0 ± 3.6 [10^{11} W/cm^2], respectively. This represents a scaling of ablation depth with laser intensity to the (5/9)th power, as seen in Fig. 6.

The mass ablation rate is determined from the ablation depth by the relation $\dot{m}=d_a\rho/\tau_L$, where ρ is the density of the target material (7.31 g/cm^3 for Sn), and τ_L is the laser pulse duration. Because the scaling of mass ablation rate with laser intensity found in the present work was consistent with the scaling found in previous studies in overlapping parameter space, it will be assumed that the scaling of mass ablation rate with laser wavelength and target atomic number are also equivalent to those found in the previous studies.[7,9] Under this assumption, a numerical approximation for the mass ablation rate can be written,

$$\dot{m} \approx (3.0 \times 10^3) \times \left(\frac{I_a}{10^{11}\ \mathrm{W/cm^2}}\right)^{5/9} \left(\frac{\lambda_L}{1\ \mu\mathrm{m}}\right)^{-4/9} Z^{3/8} \quad \left[\frac{\mathrm{g}}{\mathrm{cm^2\ s}}\right], \qquad (1)$$

which is consistent with the numerical approximation found in Dahmani and Kerda[9] in overlapping parameter space to within 15%. This is an indication that the scaling of mass ablation rate with target atomic number found in Dahmani and Kerdja[9] using targets with a maximum Z of 14 is valid to the much higher Z of 50 used in the present experiment.

The numerical approximation found in the present study is inconsistent with that found in Fujioka *et al.*,[10] from which a numerical approximation for mass ablation rate in the same form as Eq. (1) can be derived where the numerical factor would be 650. Therefore, under equivalent conditions, (laser intensity, laser wavelength, and target atomic number) the present work predicts the ablation depth would be approximately 4.5 times greater than predicted by the numerical approximation in Fujioka *et al.*[10] This distinction in mass ablation rate may result from the influence of the laser focal diameter, which is different by an order of magnitude in the two studies. This effect has not been examined in the vast studies of mass ablation rate for the laser fusion application, as these studies all typically use focal diameters in the range 50–100 μm.[6–9] For the case of the present work, in which the laser focal diameter is small compared to that used by Fujioka *et al.*[10] (56 versus 500 μm), the component of plasma expansion in the focal plane will be greater, which occurs when the plasma scale length ($n_e/|\nabla n_e|$) is comparable to the laser focal diameter, where n_e is the plasma electron density. In this case, the plasma exhibits a complex two dimensional expansion,[18] whereas in the case where the laser focal diameter is large compared to the plasma scale length the expansion is one dimensional and directed along the target normal. The case in which the plasma expands one dimensionally will restrict the ablation during the laser pulse and thus the mass ablation rate should be lower, as observed in the experiments.

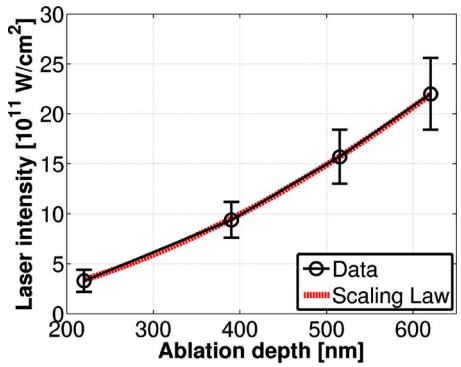

FIG. 6. (Color online) Variation of ablation depth with laser intensity, and comparison with a (5/9)th power fit.

V. CONCLUSIONS

Spectroscopic and particle diagnostics generated consistent measurements of the ablation depth in a Sn laser-produced plasma in the intensity range 3×10^{11} to 2×10^{12} W/cm^2, which is relevant to the extreme ultraviolet light source application. It was found that ablation depth scales with laser intensity to the (5/9)th power, which is consistent with a theoretical model of steady-state laser ablation in which energy deposition occurs by nonlocalized collisional absorption before the critical density, and the energy transport to the ablation front is by diffusive conduction of thermal electrons.[5,13] The numerical approximation found in

the experiments agreed with previous studies of mass ablation rate in overlapping parameter space[7,9] to within 15%, and the scaling with target atomic number found in these previous studies was found to remain valid to the high atomic number of the target used in the present experiments. The numerical approximation generated in the present experiment was found to be inconsistent with another previous study in a similar parameter space,[10] and the difference was attributed to the effects on the plasma expansion of the focal spot diameter, which was different by an order of magnitude in the two experiments.

[1]J. Benschop, V. Banine, S. Lok, and E. Loopstra, J. Vac. Sci. Technol. B **26**, 2204 (2008).
[2]C. W. Gwyn, R. Stulen, D. Sweeney, and D. Attwood, J. Vac. Sci. Technol. B **16**, 3142 (1998).
[3]S. Namba, S. Fujioka, H. Nishimura, Y. Yasuda, K. Nagai, N. Miyanaga, Y. Izawa, K. Mima, and K. Takiyama, Appl. Phys. Lett. **88**, 171503 (2006).
[4]Y. Tao, M. S. Tillack, S. S. Harilal, K. L. Sequoia, and F. Najmabadi, Appl. Phys. Lett. **101**, 023305 (2007).
[5]M. H. Key, *The Physics of Laser Plasma* (North-Holland, Amsterdam, 1991).
[6]R. Fabbro, E. Fabre, F. Amiranoff, C. Garban-Labaune, J. Virmont, M. Weinfeld, and C. E. Max, Phys. Rev. A **26**, 2289 (1982).
[7]A. Ng, D. Pasini, P. Celliers, D. Parfeniuk, L. Da Silva, and J. Kwan, Appl. Phys. Lett. **45**, 1046 (1984).
[8]F. Dahmani, J. Appl. Phys. **74**, 622 (1993).
[9]F. Dahmani and T. Kerdja, Laser Part. Beams **9**, 769 (1991).
[10]S. Fujioka, H. Nishimura, K. Nishihara, M. Murakami, Y.-G. Kang, Q. Gu, K. Nagai, T. Norimatsu, N. Miyanaga, Y. Izawa, K. Mima, Y. Shimada, A. Sunahara, and H. Furukawa, Appl. Phys. Lett. **87**, 241503 (2005).
[11]P. Mora, Phys. Fluids **25**, 1051 (1982).
[12]R. Fabbro, C. E. Max, and E. Fabre, Phys. Fluids **28**, 1463 (1985).
[13]F. Dahmani and T. Kerdja, Phys. Fluids B **3**, 1232 (1991).
[14]M. C. Schurmann, T. Missalla, K. Mann, S. Kranzusch, R. M. Klein, F. Scholze, G. Ulm, R. Lebert, and L. Juschkin, Proc. SPIE **5037**, 378 (2003).
[15]E. Woryna, P. Parys, J. Wołowski, and W. Mróz, Laser Part. Beams **14**, 293 (1996).
[16]S. Fujioka, H. Nishimura, K. Nishihara, A. Sasaki, A. Sunahara, T. Okuno, N. Ueda, T. Ando, Y. Tao, Y. Shimada, K. Hashimoto, M. Yamaura, K. Shigemori, M. Nakai, K. Nagai, T. Norimatsu, T. Nishikawa, N. Miyanaga, Y. Izawa, and K. Mima, Phys. Rev. Lett. **95**, 235004 (2005).
[17]R. C. Spitzer, R. L. Kauffman, T. Orzechowski, D. W. Phillion, and C. Cerjan, J. Vac. Sci. Technol. B **11**, 2986 (1993).
[18]K. Sequoia, Y. Tao, S. Yuspeh, R. Burdt, and M. S. Tillack, Appl. Phys. Lett. **92**, 221505 (2008).